Applied Catalysis B: Environmental 91 (2009) 113–122

Contents lists available at ScienceDirect

Applied Catalysis B: Environmental

journal homepage: www.elsevier.com/locate/apcatb

Selective catalytic reduction of NO by ethanol: Speciation of iron and "structure–properties" relationship in FeSiBEA zeolite

Janusz Janas [a,*], Jacek Gurgul [a], Robert P. Socha [a], Tetsuya Shishido [b], Michel Che [c,d,e], Stanislaw Dzwigaj [c,d,**]

[a] Institute of Catalysis and Surface Chemistry, Polish Academy of Sciences, ul. Niezapominajek 8, 30-239 Kraków, Poland
[b] Department of Molecular Engineering, Kyoto University, 615-8510 Kyoto, Japan
[c] UPMC Univ Paris 6, UMR 7197, Laboratoire de Réactivité de Surface, 4 Place Jussieu, 75252 Paris Cedex 05, France
[d] CNRS, UMR 7197, Laboratoire de Réactivité de Surface, 4 Place Jussieu, 75252 Paris Cedex 05, France
[e] Institut Universitaire de France, France

ARTICLE INFO

Article history:
Received 7 April 2009
Received in revised form 2 May 2009
Accepted 10 May 2009
Available online 19 May 2009

Keywords:
BEA
Zeolite
Iron
SCR
NO
Ethanol
XRD
UV–vis
XPS
XAS
IR
Catalysis

ABSTRACT

The speciation of iron in FeSiBEA zeolites is investigated in order to evidence the "structure–properties" relationship in the selective catalytic reduction (SCR) of NO by ethanol. Fe_xSiBEA zeolites are prepared in acidic (pH 2.5) (x = 0.3, 0.9 and 4.2 Fe wt%) or basic (pH 10) (x = 3.6 Fe wt%) conditions by a two-step postsynthesis method which allows to incorporate Fe into zeolite, as evidenced by XRD. For low Fe content ($Fe_{0.3}$SiBEA, $Fe_{0.9}$SiBEA), iron incorporated as Fe(III) ions generates Brønsted acidic sites as shown by FTIR of pyridine. Framework tetrahedral Fe(III) ions are evidenced by diffuse reflectance UV–vis, XANES and EXAFS. For higher Fe content ($Fe_{4.2}$SiBEA), beside tetrahedral Fe(III) ions which are dominant, octahedral Fe(III) species are also present as shown by DR UV–vis, XPS and EXAFS. In contrast, for $Fe_{3.6}$SiBEA prepared in basic condition (pH 10), an extra-framework Fe(III) oxide phase is mainly observed.

The catalytic activity of Fe_xSiBEA in the SCR of NO by ethanol strongly depends on the speciation of iron and a structure–properties relationship has been evidenced. $Fe_{0.3}$SiBEA and $Fe_{0.9}$SiBEA which mainly contain framework tetrahedral Fe(III) ions are active, with selectivity toward N_2 exceeding 90% for NO conversion from 25% to 55%. When additional octahedral Fe(III) species are present ($Fe_{4.2}$SiBEA), the full oxidation of ethanol and NO by O_2 becomes important, with CO_2 and NO_2, respectively, appearing at the expenses of N_2. The NO conversion linearly depends on Fe concentration assuming a first order reaction, suggesting that tetrahedral and octahedral Fe(III) species are well dispersed, as confirmed by XRD. The iron oxide phase is quite inactive, the activity and selectivity of $Fe_{3.6}$SiBEA being governed by the small amount of tetrahedral Fe(III) ions.

1. Introduction

Iron zeolites are active in several reactions, including N_2O decomposition [1–4], selective catalytic reduction of NO_x and N_2O [5,6] and selective oxidation of different substrates [7–10]. Fe-ZSM-5 has been the most studied system and its preparation, characterization and catalytic activity have been largely investigated [11–16]. Recently [17,18], BEA zeolite has shown to be an attractive host for iron leading to a FeBEA zeolite with improved activity in the reduction of N_2O by NH_3 in the presence of oxygen. The effect of the preparation procedure on the speciation (i.e., distribution of an element amongst defined chemical species in a system [19]) of iron and performance of Fe-BEA is still to be explored. As a matter of fact, depending on the preparation method, different iron species can be formed in zeolites: isolated framework and extra-framework Fe species, FeO_x oligomers and/or iron oxides. Several studies have aimed at assigning the activity and/or selectivity of iron zeolites to one of these species. The question of speciation is, of course, not limited to iron. Copper, nickel and cobalt zeolites have been also investigated [20–23].

The complexity of the problem can be greatly reduced if well-defined catalysts with a single type of iron species can be prepared. Because current methods for dispersing transition metals in zeolites are non-selective, a two-step postsynthesis method was developed which consists first of creating vacant T-atom sites by

* Corresponding author. Fax: +48 12 4 25 19 23.
** Corresponding author at: UPMC Univ Paris 6, UMR 7197, Laboratoire de Réactivité de Surface, 4 Place Jussieu, 75252 Paris Cedex 05, France. Fax: +33 1 44 27 60 33.
E-mail addresses: ncjanas@cyf-kr.edu.pl (J. Janas), stanislaw.dzwigaj@upmc.fr (S. Dzwigaj).

0926-3373/$ – see front matter © 2009 Elsevier B.V. All rights reserved.
doi:10.1016/j.apcatb.2009.05.013

dealumination of BEA zeolite with nitric acid and then impregnating the resulting SiBEA with metal precursors [24–26].

As shown earlier [27], this postsynthesis method allows, for low metal content (0.3 and 0.9 Fe wt%), to incorporate iron mainly as isolated and homogeneously distributed tetrahedral Fe(III) species without formation of FeO_x oligomers or iron oxide as shown by diffuse reflectance UV–vis, EPR and Mössbauer. For higher iron content (4.2 Fe wt%), diffuse reflectance UV–vis and Mössbauer investigations revealed that, beside the main framework tetrahedral and octahedral Fe(III) ions, some amount of extra-framework FeO_x oligomers and superparamagnetic Fe-oxyhydroxide is present. For $Fe_{3.6}$SiBEA, prepared in basic conditions a superparamagnetic Fe-oxyhydroxide is detected by Mössbauer spectroscopy and constitutes the main phase.

In the present work, the speciation of iron in Fe_xSiBEA zeolites is investigated in order to evidence a "structure–properties" relationship in the selective catalytic reduction (SCR) of NO by ethanol. To compare the activity of various Fe_xSiBEA zeolites, the reaction of SCR of NO in excess oxygen is performed in the presence or absence of ethanol in order to evidence the reactivity of the different kinds of Fe species. Moreover, the role of NO_2 as possible intermediate is also discussed.

2. Experimental

2.1. Catalyst preparation

Fe_xSiBEA catalysts (x = 0.3, 0.9, 4.2 Fe wt%) were prepared by the two-step postsynthesis method reported earlier for VSiBEA zeolites [24,25]. In the first step, 2 g of siliceous BEA zeolite (Si/Al > 1300) with surface area of 655 $m^2\,g^{-1}$, obtained by treatment of a tetraethyl ammonium (TEA) BEA zeolite (Si/Al = 11) (RIPP, China), were treated by a 13 mol L^{-1} HNO_3 solution under stirring (4 h, 353 K) to remove aluminium. In the second step, the resulting solids obtained after filtration were stirred for 24 h at 298 K in aqueous solutions (pH 2.5) containing from 0.36×10^{-3} to 1.8×10^{-2} mol L^{-1} of $Fe(NO_3)_3{\cdot}9H_2O$. The suspensions formed were further stirred for 2 h in air at 353 K until complete evaporation of water. The solids were then washed three times with distilled water and finally dried in air at 353 K for 24 h. The solids with 0.3, 0.9 and 4.2 Fe wt% were labelled $Fe_{0.3}$SiBEA, $Fe_{0.9}$SiBEA $Fe_{4.2}$SiBEA, respectively. The samples $Fe_{0.3}$SiBEA and $Fe_{0.9}$SiBEA with surface area of 650 and 640 $m^2\,g^{-1}$, respectively were white while $Fe_{4.2}$SiBEA with surface area of 620 $m^2\,g^{-1}$ was bright brown.

The sample $Fe_{3.6}$SiBEA with surface area of 400 $m^2\,g^{-1}$ also brown was prepared by the procedure described above but using, in the second step, a basic $Fe(NO_3)_3$ solution (pH 10, $c = 1.8 \times 10^{-2}$ mol L^{-1}) obtained by adding ammonia.

These samples were characterized by different techniques, after particular treatments described in the next section.

2.2. Catalyst characterization

Chemical analysis of iron was performed with inductively coupled plasma atom emission spectroscopy at the CNRS Centre of Chemical Analysis (Vernaison, France).

Powder X-ray diffractograms (XRD) were recorded at ambient atmosphere on a Siemens D5000 using the Cu Kα radiation (λ = 154.05 pm).

Diffuse reflectance UV–vis (DR UV–vis) spectra were recorded at ambient atmosphere on a Cary 5E spectrometer equipped with an integrator and a double monochromator.

Transmission FTIR spectra of self-supported wafers, with diameter of 12 mm introduced into an *in situ* IR cell equipped with CaF_2 windows, were recorded at room temperature on a PerkinElmer Spectrum One spectrometer with a resolution of 2 cm^{-1} after calcination at 773 K for 3 h in flowing dry air and then outgassing to 10^{-3} Pa at 573 K. The number of scans was 32.

Those wafers were contacted with gaseous pyridine *via* a separate cell containing liquid pyridine. Physisorbed pyridine was outgassed to 10^{-3} Pa at 423, 473, 523 and 573 K.

X-ray photoelectron spectroscopy (XPS) measurements were performed with a hemispherical analyzer (SES R4000, Gammadata Scienta) using Al Kα (1486.6 eV) or Mg Kα (1253.6 eV) radiation. The pressure in the XPS chamber was around 10^{-9} mbar. The power of the X-ray source was 300 W and the energy pass for analyzer was 100 eV, corresponding to a full width at half maximum (FWHM) of 0.9 eV for the Ag $3d_{5/2}$ peak. The area of the sample analyzed was approximately 3 mm^2. The powder samples were pressed into indium foil and mounted on a special holder. The binding energy (BE) for Si, O and Fe was measured by taking the C_{1s} peak at 285.0 eV as internal standard, with an error of ±0.2 eV for BE values. Before recording XP spectra, the catalysts were evacuated at 10^{-9} mbar in the XPS analyzer chamber. All spectra were fitted with a Voigt function (a composition 70/30 of Gaussian and Lorentz function) in order to determine the number of components under each XPS peak.

X-ray absorption spectra (XAS) were recorded on the beam line BL-9A at the Photon Factory of the Institute of Materials Structure Science for High Energy Accelerator Research Organization at Tsukuba, Japan (Proposal No. 2007G127). Fe K-edge XANES and EXAFS spectra were recorded in a transmission mode at room temperature by using two ion chambers (N_2 (I_0) and 85% N_2 diluted with Ar (I)). Si(1 1 1) single crystal was used to obtain a monochromatic X-ray beam. Analysis of EXAFS data were performed using the REX2000 program (Version 2.5.7, Rigaku Corp.). For EXAFS analysis, the oscillation was first extracted from EXAFS data using a spline smoothing method [28]. The oscillation was normalized by the edge height around 70–100 eV above the threshold. Fourier transforms (FT) of k^3-weighted EXAFS spectra were obtained over a k-range of 3.5–14.0 $Å^{-1}$. Fourier transformed data for each peak were analyzed by a curve-fitting method, using theoretical phase shifts and amplitude functions derived from the FEFF8.2 program [29].

2.3. Catalytic properties measurements

Before the catalytic test, the samples were heated up to 523 K in oxygen/helium mixture and then NO and ethanol vapour streams were switched on. The standard conditions were: 2 h runs at 523–623 K and 1 h runs at higher reaction temperature. NO_x and CO_x concentrations at the reactor outlet were continuously monitored to check if pseudo steady-state conditions were established. The reaction temperature was increased every 50 K interval up to 773 K, and then lowered in the same way to 523 K. In the case of NO conversion or product selectivity measurements, the heating sequence was repeated to obtain real steady-state reaction conditions in the reaction temperature range. Only for NO oxidation experiments in absence of ethanol, heating of the catalysts in a mixture containing 2 vol.% O_2 in He at 723 K for 1 h was necessary in order to obtain a reproducible activity.

The activity of catalysts in the SCR of NO by ethanol was measured in a conventional flow reactor coupled to an analytical system. A gas chromatograph (CHROM-5) provided with TCD and FID detectors was used for analysis of gas-phase products. CO_2, NO and ethylene were separated with a 8 ft × 1/8 in. nickel HayeSep R column (Alltech) at 333 K. O_2, N_2 and CO were separated by a stainless steel 2 m × 3 mm MS 5A column (Supelco) at the same temperature. Ethanol and other organic compounds (mainly ethylene, acetaldehyde, acetic acid, acetonitrile, and, in minor quantities, esters and other hydrocarbons) were separated with a FID detector and 2 m × 3 mm glass columns: 10% SP-1000 on 80/

100 Supelcort and 10% SP-2100 on 100/120 Supelcort, heated from 333 to 393 K. The calculations were performed with the CHROMA 2000 computer analytical program. The concentrations of O_2, NO_x and CO were monitored with a GA-60 (MADUR) flue gas analyser provided with electrochemical sensors. The NO and ethylene concentrations were additionally measured by means of a Photovac 10S50 GC with KCl–alumina column (at 313 K) provided with a photoionization detector. The presence among reaction products of active intermediates such as ammonia, HCN and HNCO was detected by a FTIR multichannel GASMET DX-4000 analyzer (resolution: 7.72 cm^{-1}, optical length: 500 cm, scan time 60 s).

The composition of the feed was 1000 ppm NO, 1000 ppm ethanol, a mixture of 2 vol.% O_2 in He with a catalyst volume of 1 mL (~0.52 g) and a 10,000 h^{-1} gas hour space velocity. All conversion and selectivity values were presented in mol.%. Because of the difficulty to determine N_2 concentrations at the reactor outlet, the selectivity toward N_2 was determined as follows:

$$S_{N_2} = 100 - (S_{NO_2} + S_{N_2O} + S_{NH_3} + S_{OrgN})\,(\%)$$

where S_{NO_2}, S_{N_2O} and S_{NH_3} is the selectivity toward NO_2, N_2O and ammonia, respectively and S_{OrgN} is the sum of selectivities toward nitrogen-containing organic compounds.

3. Results and discussion

3.1. Incorporation of iron into the framework of dealuminated BEA

3.1.1. X-ray diffraction and FTIR spectroscopy

Fig. 1 shows the XRD patterns of AlBEA, SiBEA and Fe_xSiBEA which all are typical of BEA zeolite. The crystallinity is preserved after dealumination and the samples do not show any evidence of extra framework crystalline compounds or long-range amorphization of the zeolite. The decrease of the $d_{3\,0\,2}$ spacing related to the narrow main diffraction peak near 22–23° from 3.942 (AlBEA) (with 2θ of 22.55°) to 3.912 Å (SiBEA) (with 2θ of 22.71°) upon dealumination indicates contraction of the matrix as a result of removal Al atoms, in line with earlier data [24–26,30,31]. In contrast, the significant increase to 3.939 (with 2θ of 22.64°) and 3.941 Å (with 2θ of 22.61°) upon introduction of 0.9 and 4.2 Fe wt%, respectively into SiBEA indicates expansion of the matrix as already reported for VSiBEA zeolites [24–26]. The progressive increase of the $d_{3\,0\,2}$ spacing with Fe content is taken as evidence of the incorporation of Fe into the framework.

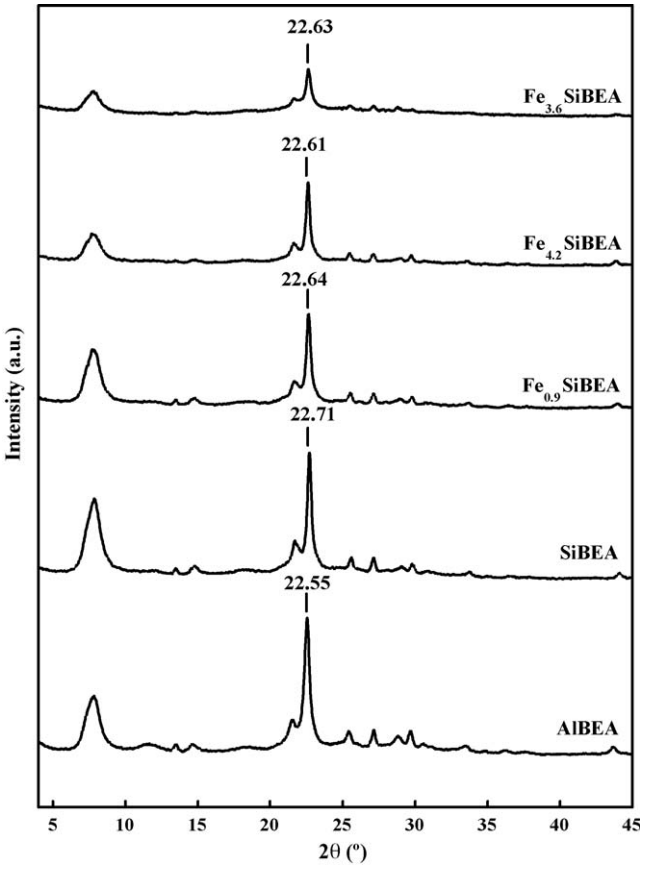

Fig. 1. XRD patterns recorded at ambient atmosphere of AlBEA, SiBEA, $Fe_{0.9}$SiBEA, $Fe_{4.2}$SiBEA and $Fe_{3.6}$SiBEA as prepared.

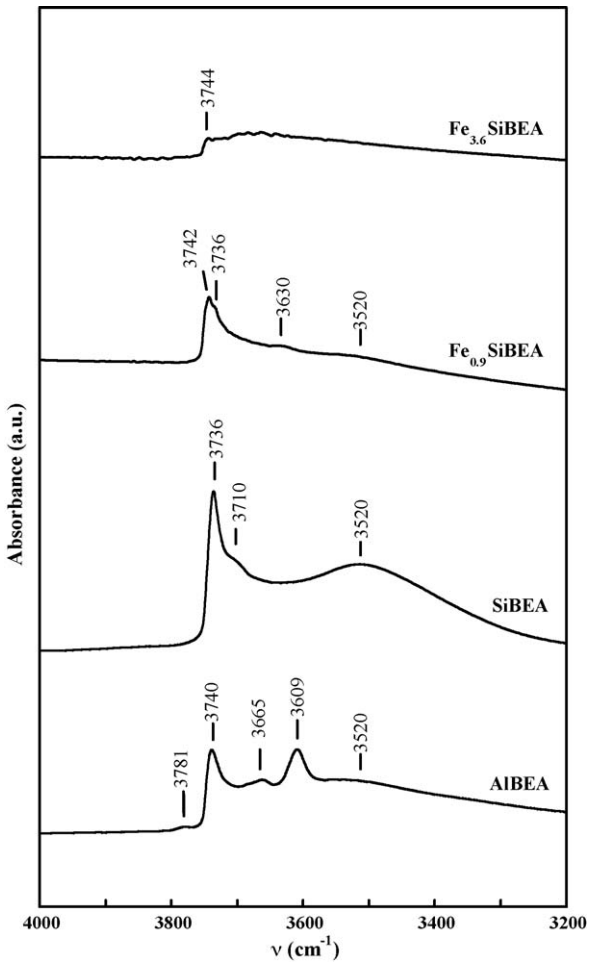

Fig. 2. FTIR spectra recorded at room temperature of AlBEA, SiBEA, $Fe_{0.9}$SiBEA and $Fe_{3.6}$SiBEA after calcination at 773 K for 3 h in flowing air following by outgassing at 10^{-3} Pa for 2 h at 573 K.

$Fe_{3.6}$SiBEA exhibits much less intense diffraction lines than SiBEA and $Fe_{0.9}$SiBEA, suggesting that basic conditions involved in the sample preparation affect the crystallinity.

The treatment of AlBEA zeolite with aqueous HNO_3 solution involves the elimination of Al atoms from the framework as evidenced by the disappearance of IR bands at 3781, 3665 attributed to AlO–H and 3609 cm^{-1} to Al–O(H)–Si groups (Fig. 2), in line with earlier investigations [24,25]. The appearance of narrow bands at 3736 and 3710 cm^{-1} related to isolated silanol groups and of a broad band at 3520 cm^{-1} due to H-bonded SiOH groups in SiBEA reveals the presence of vacant T-sites associated with silanol groups (Fig. 2), as reported earlier by Dzwigaj et al. [24,25].

The incorporation of Fe into SiBEA zeolite leading to Fe_xSiBEA induces a reduction of intensity of these bands as shown in Fig. 2

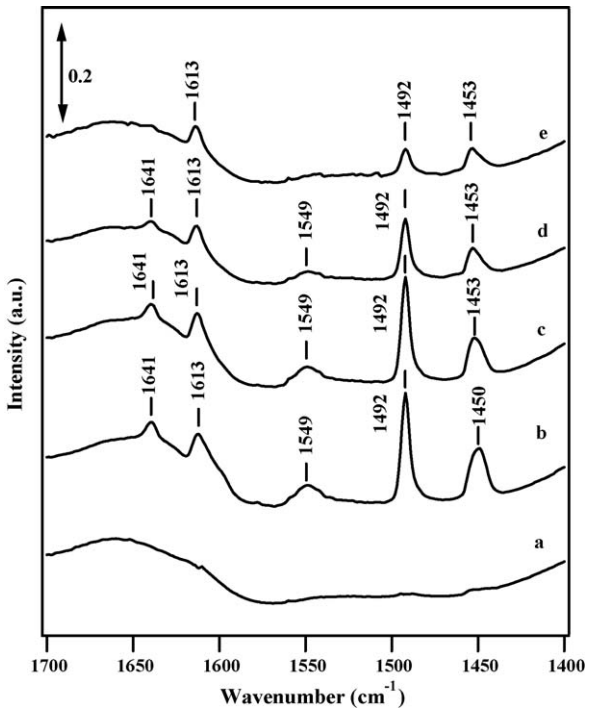

Fig. 3. FTIR spectra recorded at room temperature of $Fe_{0.9}$SiBEA (a) after calcination at 773 K for 3 h in flowing air followed by outgassing to 10^{-3} Pa at 573 K, (b) after adsorption of pyridine at room temperature on sample (a), followed by outgassing of excess pyridine at 423, (c) 473, (d) 523 and (e) 573 K to 10^{-3} Pa.

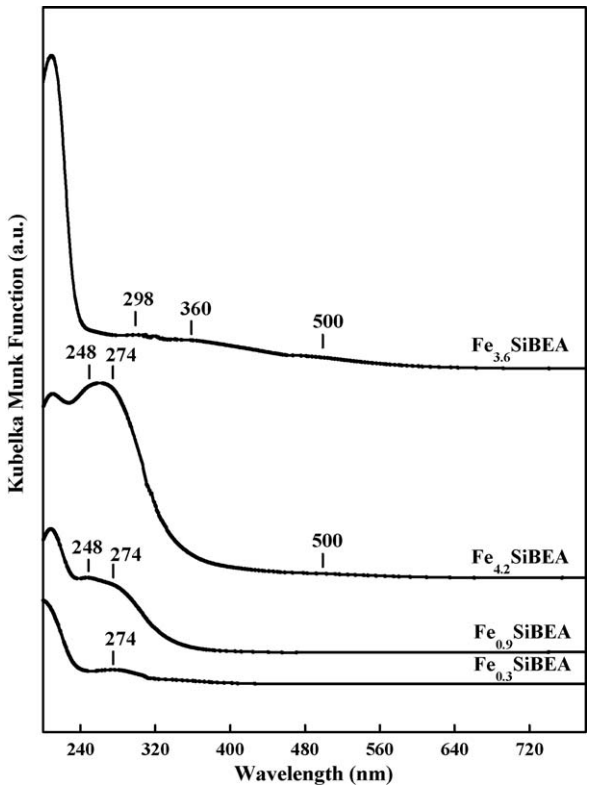

Fig. 4. DR UV–vis spectra recorded at ambient atmosphere of $Fe_{0.3}$SiBEA, $Fe_{0.9}$SiBEA, $Fe_{4.2}$SiBEA and $Fe_{3.6}$SiBEA as prepared.

for $Fe_{0.9}$SiBEA, suggesting that SiO–H groups of vacant T-sites reacts with Fe ions with formation of framework Fe(III) sites. It is confirmed by appearance of the IR band at 3630 cm^{-1} which can be attributed to ≡Fe(III)–O(H)–Si≡ acidic sites. The similar phenomenon has been earlier observed by some of us upon incorporation of chromium into SiBEA zeolite with formation of ≡Cr(III)–O(H)–Si≡ acidic sites [32]. In contrast, isolated SiO–H groups present outside of vacant T-sites, observed also in the IR band of AlBEA at about 3740 cm^{-1}, do not react with Fe ions and are now well seen in IR band of $Fe_{0.9}$SiBEA at 3742 cm^{-1}.

For $Fe_{3.6}$SiBEA prepared in basic condition (pH 10), the IR band at 3630 cm^{-1} is not observed (Fig. 2) as well as the other IR bands of OH groups suggesting that, not only incorporation of Fe ions into the framework sites do not take place but also some destruction of crystalline structure occur. It is in line with strong decreasing of the surface area of BEA zeolite observed after introduction of Fe ions into SiBEA in basic condition. The surface area decreases from 655 $m^2\ g^{-1}$ (SiBEA) to 400 $m^2\ g^{-1}$ ($Fe_{3.6}$ SiBEA).

Fig. 3 shows the FTIR spectra of $Fe_{0.9}$SiBEA after calcination at 773 K in air for 3 h, then outgassing at 573 K (10^{-3} Pa) (Fig. 3a) followed by adsorption of pyridine at room temperature and further outgassing at 423 (Fig. 3b), 473 (Fig. 3c), 523 (Fig. 3d) and 573 K (Fig. 3e). Bands typical of pyridinium cations are observed at 1549 and 1641 cm^{-1}, indicating a small amount of Brønsted acidic sites. These data suggest that ≡Fe(III)–O(H)–Si≡ acidic sites are formed upon outgassing $Fe_{0.9}$SiBEA. Similar results were found for CrSiBEA zeolite [32]. The other bands at about 1613, 1492 and 1450–1453 cm^{-1} observed (Fig. 3b–e) correspond to pyridine interacting with Lewis acidic sites, in line with earlier data on CrSiBEA [32], SiBEA and VSiBEA [33,34]. Pyridinium cations (bands at 1549 and 1641 cm^{-1}) and pyridine bonded to Lewis acidic sites (bands at 1610, 1491 and 1450–1453 cm^{-1}) remain even after outgassing at 573 K (Fig. 3d and e), suggesting the presence of strong Brønsted and Lewis acidic sites in $Fe_{0.9}$SiBEA.

3.2. Dependence of the speciation of iron on Fe content

3.2.1. Diffuse reflectance UV–vis spectroscopy

Fig. 4 shows the DR UV–vis spectra of Fe_xSiBEA samples. The white $Fe_{0.3}$SiBEA and $Fe_{0.9}$SiBEA samples exhibit one band at 274 nm and two bands at 248 and 274 nm, respectively, assigned to oxygen-to-metal charge transfer (CT) transitions involving tetrahedral Fe(III) ions, in line with earlier results [35–42]. The absence of a broad band near 500 nm, suggests that FeO_x oligomers are not present [35–37]. For higher Fe content ($Fe_{4.2}$SiBEA), bands in the 220–300 and 310–550 nm ranges are observed which can be assigned to tetrahedral Fe(III) and octahedral Fe(III), respectively, in line with earlier studies [16]. For $Fe_{3.6}$SiBEA prepared in basic solution, large bands at 360 and 500 nm are mainly observed suggesting that an extra-framework iron oxide phase becomes predominant, consistent with the brown color of the sample.

3.2.2. X-ray photoelectron spectroscopy

XPS measurements of fresh (as prepared and conditioned in dry flowing air at 453 K for 3 h) or used (just after catalytic test and conditioned in dry flowing air at 453 K for 3 h) Fe_xSiBEA were analyzed in the BE regions of Si 2p, Al 2p, Fe 2p, O 1s and C 1s.

The Si 2p BE value (103.6 eV) close to that reported earlier for BEA, MFI and MOR zeolites [42–46] is related to the presence of tetrahedral Si(IV). The O 1s line can be decomposed (results not shown) into three components: a main peak at 533.1 eV (assigned to oxygen of zeolite framework), a smaller peak (2–3% of the total O 1s intensity) at ~530.7 eV due to oxygen–metal bonds and a peak at 534–535 eV assigned to adsorbed water and/or oxygen of organic contaminants. The C 1s core line is composed of three peaks at 285.0 eV (organic contaminants), 287.2 eV (CO groups) and 289.8 eV (carbonates).

As shown in Figs. 5–7, in the Fe 2p range of used and fresh Fe_xSiBEA, each peak (Fe $2p_{3/2}$ and Fe $2p_{1/2}$) can be decomposed into

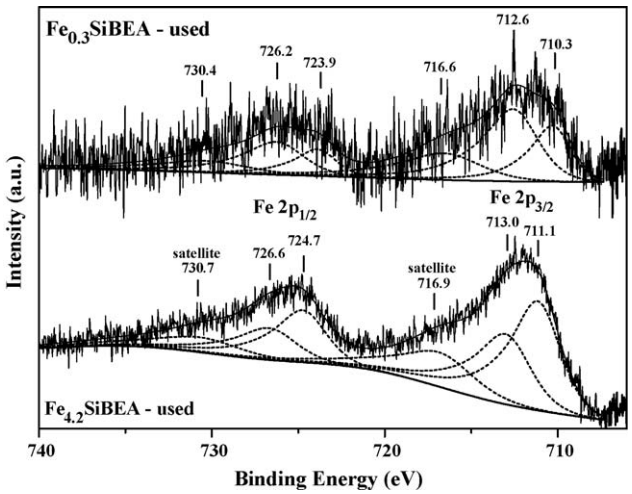

Fig. 5. XP spectra recorded at room temperature of Fe_{2p} of fresh and used $Fe_{0.3}$SiBEA.

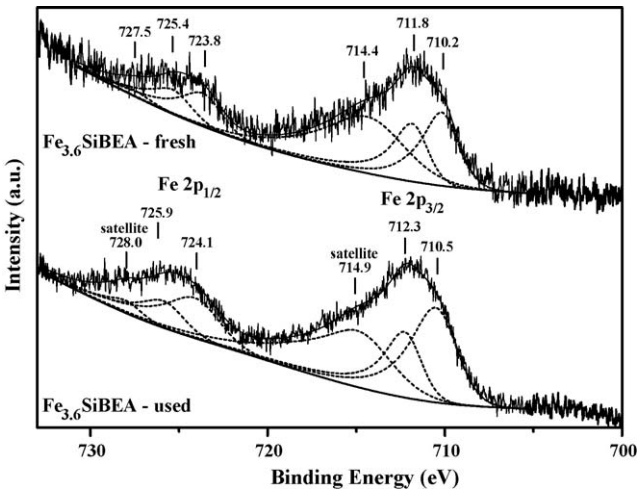

Fig. 7. XP spectra recorded at room temperature of Fe_{2p} of fresh and used $Fe_{3.6}$SiBEA.

a doublet and one broad asymmetric satellite. The Fe $2p_{3/2}$ doublet is at ~710 eV and the second at ~712 eV. These values, characteristic of Fe(III), vary from 710.2–710.6 (for FeOOH) to 713.25 eV (for $Fe_2(SO_4)_3$), with intermediate values for ferrihydrite ($Fe_2O_3{\cdot}2FeOOH{\cdot}2.6H_2O$) (710.8 eV) and α-Fe_2O_3 (710.6–711.5 eV) [47–50].

The presence of Fe(III) in $Fe_{0.9}$SiBEA, $Fe_{4.2}$SiBEA and $Fe_{3.6}$SiBEA is confirmed by the charge transfer satellite of Fe $2p_{3/2}$ at ~715 eV and of Fe $2p_{1/2}$ at ~729 eV [47] and by the value of the Fe $2p_{3/2}$–Fe $2p_{1/2}$ splittings of ~13.6 eV [51].

However, as reported earlier [47,52,53], it is difficult, using XPS only, to determine the oxidation state of iron, even taking into account the charge transfer satellites of Fe $2p_{3/2}$ and Fe $2p_{1/2}$ peaks. Indeed, the Fe$2p_{3/2}$ and Fe$2p_{1/2}$ satellites, which appear at 713.8–716.9 and 727.4–730.7 eV, respectively, could indicate the presence of Fe(II). However, Mössbauer evidences that iron in Fe_xSiBEA zeolites [27] is mainly present as isolated tetrahedral Fe(III) for low Fe content ($Fe_{0.3}$SiBEA and $Fe_{0.9}$SiBEA), with additional octahedral Fe(III) at higher Fe content ($Fe_{4.2}$SiBEA). For $Fe_{3.6}$SiBEA, Fe-oxyhydroxide (ferrihydrite) is mainly detected.

Thus, on the basis of XPS and Mössbauer data, Fe_xSiBEA exhibit different types of Fe(III) which relative amounts depend on Fe content and preparation conditions, in line with earlier DR UV–vis and EPR data [27]. The doublets which appear in the XP spectra of Fe_xSiBEA could be related to different types of Fe(III) ions (tetrahedral and octahedral) as mentioned above.

The shape of the Fe 2p spectra of used $Fe_{0.9}$SiBEA and $Fe_{3.6}$SiBEA zeolites does not change significantly (Figs. 6 and 7), with only a slight shift of the peaks to higher BE, suggesting that similar Fe(III) ions are present in fresh and used catalysts.

Literature data also give information on the nature and oxidation state of Fe in Fe-containing zeolites. For Fe-ZSM-5 catalyst with low Fe content (~0.3 Fe wt%), it was claimed that the calcined zeolite contains both isolated Fe(III) ions and small Fe(III) oxide nanoclusters [11] but only one Fe $2p_{3/2}$ peak at 711.7–712.0 eV was found, close to values observed for our catalysts. We assign the Fe $2p_{3/2}$ peak to lattice Fe(III) ions bound to oxygen. The second peak, at about 711 eV, appears for samples with higher Fe content (~3 Fe wt%).

XPS results on Fe_xSiBEA and literature data do not allow to draw conclusions as univocal as in the case of their Co_xSiBEA analogues investigated earlier [43]. While two types of Fe(III) species are evidenced, it is difficult to conclude whether they are tetrahedral or octahedral.

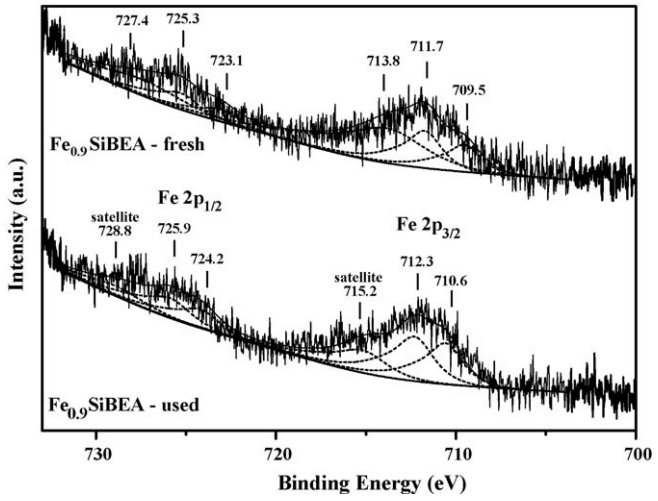

Fig. 6. XP spectra recorded at room temperature of Fe_{2p} of fresh and used $Fe_{0.9}$SiBEA.

3.2.3. XANES

Fig. 8 shows the Fe K-edge XANES spectra of reference compounds (ferrisilicate and α-Fe_2O_3) and Fe_xSiBEA samples as-prepared. Fe species are tetrahedral in ferrisilicate, and octahedral in α-Fe_2O_3. The pre-edge peak at ~7114 eV, assigned to the 1s–3d dipolar transition, is sensitive to the electronic and geometric structures of iron. This forbidden transition generally gains intensity when Fe ion loses its inversion center upon temperature-dependent distortion or is tetrahedral (mixing of 3d and 4p orbitals). Although, the intensity of this pre-edge peak is expected to increase as follows: $I_{\text{octahedral}} < I_{\text{square pyramidal}} < I_{\text{tetrahedral}}$ (Fig. 8) [54,55], it is however weak, even for tetrahedral Fe ions. The same holds true for tetrahedral Co(II) in CoAPO-5 [56].

Ferrisilicate, with tetrahedral Fe(III), exhibits the highest intensity, whereas α-Fe_2O_3 with distorted octahedral Fe(III) ions exhibits a very weak and broad absorption. Among the samples, $Fe_{0.9}$SiBEA exhibits the most intense pre-edge peak which is however slightly weaker than that of ferrisilicate with MFI structure. The pre-edge peak intensity for $Fe_{3.6}$SiBEA and $Fe_{4.2}$SiBEA samples is lower than that for ferrisilicate, and higher than that for α-Fe_2O_3. The oscillation observed for $Fe_{0.9}$SiBEA at high energy (~15 eV above the absorption edge) is almost similar to that of ferrisilicate. These results confirm that Fe in $Fe_{0.9}$SiBEA is

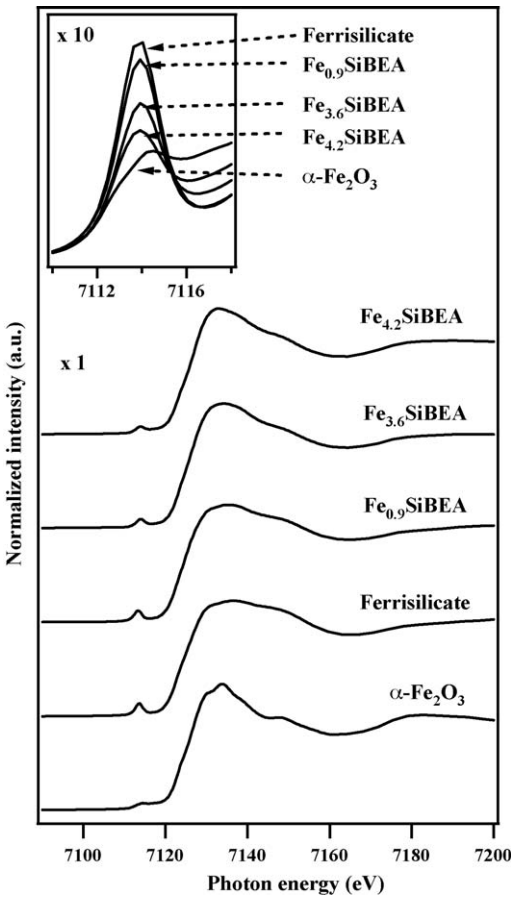

Fig. 8. Fe K-edge XANES spectra recorded at room temperature of α-Fe_2O_3 and ferrisilicate references and $Fe_{0.9}$SiBEA, $Fe_{3.6}$SiBEA and $Fe_{4.2}$SiBEA as prepared.

mainly present as tetrahedral Fe(III), while it is in higher coordination, probably octahedral in $Fe_{3.6}$SiBEA and $Fe_{4.2}$SiBEA.

3.2.4. EXAFS

Fig. 9 shows k^3-weighted EXAFS spectra and Fourier transforms (not phase shift-corrected) of reference compounds (ferrisilicate and α-Fe_2O_3) and Fe_xSiBEA samples as-prepared. The oscillations of $Fe_{0.9}$SiBEA similar to those of ferrisilicate are different from those of $Fe_{3.6}$SiBEA and $Fe_{4.2}$SiBEA, indicating different local environments of Fe. The peak at ~1.5 Å can be assigned to the contribution of the Fe–O shell, in line with previous work [54]. It should be noted that Fe–Fe interactions detected in α-Fe_2O_3 at ~2.8 Å, are not observed for $Fe_{0.9}$SiBEA and ferrisilicate, suggesting that Fe(III) ions are isolated in both cases. Table 1 gives the results of the curve-fitting analysis for the first coordination sphere.

For $Fe_{0.9}$SiBEA, the Fe–O distance (1.84 Å) and coordination number of Fe (4.0) are similar to those of ferrisilicate, suggesting that presence of framework distorted tetrahedral Fe(III) ions. On the other hand, $Fe_{3.6}$SiBEA and $Fe_{4.2}$SiBEA exhibit two kinds of Fe–O shells with lengths of 1.90–1.93 and 2.04–2.10 Å and coordination numbers of 3.0 and 2.8–3.0, respectively. These parameters are similar to those found for α-Fe_2O_3. α-Fe_2O_3 exhibits two kinds of Fe–O bond length of 1.95 and 2.11 Å [57] and a coordination number of 3 for Fe [58]. The total coordination number for Fe–O shells is ~6, suggesting the presence of distorted octahedral Fe(III) ions in $Fe_{3.6}$SiBEA and $Fe_{4.2}$SiBEA.

3.3. "Structure–properties" relationship

As shown earlier [43], SiBEA is poorly active, with NO conversion below 10% in the 520–775 K range. The relatively high ethanol conversion (87.5% at 623 K) is mainly due to dehydration of ethanol to ethylene and not to alcohol oxidation. The maximum selectivity toward N_2 for SiBEA is about 85% but the yield of N_2

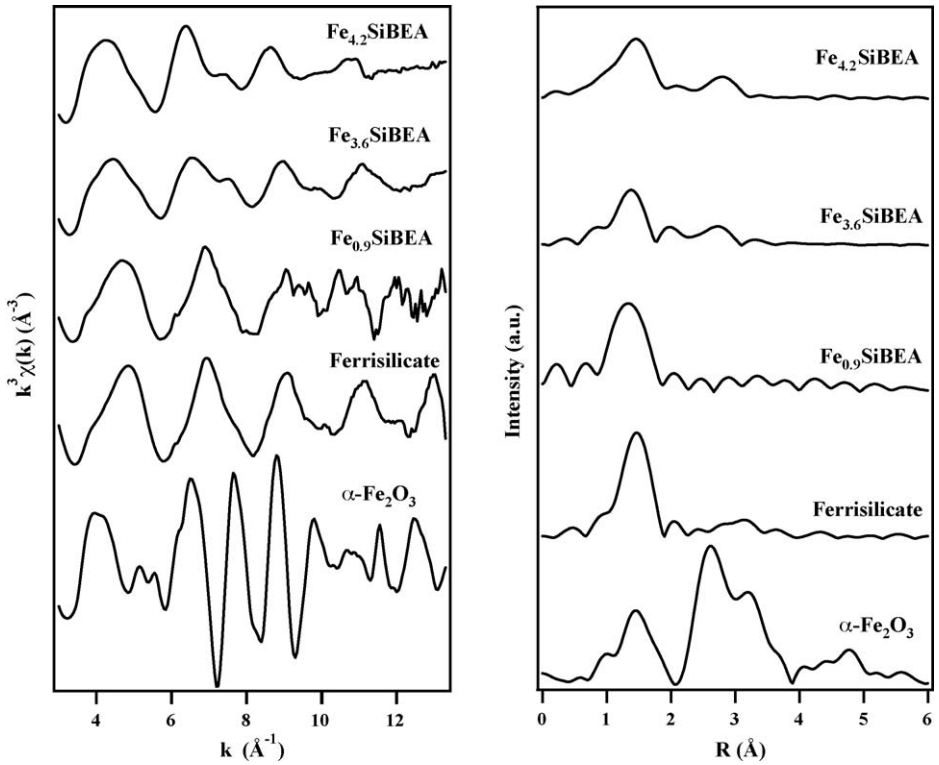

Fig. 9. k^3-Weighted EXAFS spectra and Fourier transforms (FTs) recorded at room temperature of α-Fe_2O_3 and ferrisilicate references and $Fe_{0.9}$SiBEA, $Fe_{3.6}$SiBEA and $Fe_{4.2}$SiBEA as prepared.

Table 1
Curve fitting results of Fe K-edge EXAFS spectra of α-Fe_2O_3, ferrisilicate and Fe_xSiBEA zeolites.

Sample	Shell	C.N.[a]	R (Å)[b]	σ (Å)[c]	ΔE_0 (eV)	R_f (%)
$Fe_{3.6}$SiBEA	Fe–O	3.0	1.90	0.098	3.2	2.4
	Fe–O	3.0	2.04	0.072	−12.1	
$Fe_{4.2}$SiBEA	Fe–O	3.0	1.93	0.069	−1.1	6.1
	Fe–O	2.8	2.10	0.098	6.9	
$Fe_{0.9}$SiBEA	Fe–O	4.0	1.84	0.093	−8.0	8.2
Ferrisilicate	Fe–O	3.8	1.85	0.075	−3.4	9.6
α-Fe_2O_3[d]	Fe–O	3	1.95			
	Fe–O	3	2.11			

[a] C.N. (±0.6) coordination number.
[b] R (±0.01) bond length (Å).
[c] σ (±0.02) Debye–Waller factor (Å), ΔE_0, difference in the origin of photoelectron energy between the reference and the sample (eV), R_f residual factor (%).
[d] Data on bond length were obtained by X-ray crystallography [57].

is very low, confirming that transition metal ions promote the activity. Beside N_2, NO_2 is detected in the whole temperature range.

The NO_{SCR} conversion substantially increases if SiBEA contains even a small amount of lattice tetrahedral Fe(III), as shown for $Fe_{0.3}$SiBEA (Fig. 10). The activity increases with Fe content ($Fe_{0.9}$SiBEA and $Fe_{4.2}$SiBEA) as shown by the increase of NO_{SCR} conversion (Figs. 11 and 12). The maximum of NO_{SCR} conversion for $Fe_{0.3}$SiBEA, $Fe_{0.9}$SiBEA and $Fe_{4.2}$SiBEA is 25%, 55% and 70%, respectively.

The selectivities are shown in Figs. 10–12. For $Fe_{0.3}$SiBEA, the main ethanol conversion product is ethylene at low reaction temperatures, with partial oxidation products (such as acetaldehyde, acetic acid, acetonitrile and CO) prevailing at intermediate temperatures and total oxidation product, CO_2, dominating above 700 K. The selectivity toward C_2H_4 decreases for increasing Fe content and reaction temperature. The selectivity toward organic intermediates as a function of temperature exhibits a maximum for $Fe_{0.3}$SiBEA while it decreases for $Fe_{0.9}$SiBEA and $Fe_{4.2}$SiBEA. For $Fe_{4.2}$SiBEA, this decrease is more important especially at temperatures above than 600 K when much more NO_2 is formed.

Fe_xSiBEA zeolites are selective toward N_2 with a maximum selectivity exceeding 90% for $Fe_{0.9}$SiBEA (from 550 to 775 K) (Fig. 11). For all samples, the formation of NO_2 above 600 K is accompanied with the depletion of organic products (acetaldehyde, acetic acid, acetonitrile) and CO. For $Fe_{4.2}$SiBEA, the most active sample, NO_2 formation is observed already at 575 K.

In contrast, $Fe_{3.6}$SiBEA, prepared in basic conditions and mainly containing iron oxide with chemical composition close to that of α-Fe_2O_3 [59], is far less active than $Fe_{4.2}$SiBEA, $Fe_{0.9}$SiBEA and $Fe_{0.3}$SiBEA (Fig. 13). The selectivities toward N_2, CO and organic compounds are relatively high in the whole temperature range. The formation of N_2O (not shown) and N-containing substances (mainly acetonitrile) in the 573–723 K range decreases the selectivity toward N_2 (Fig. 13).

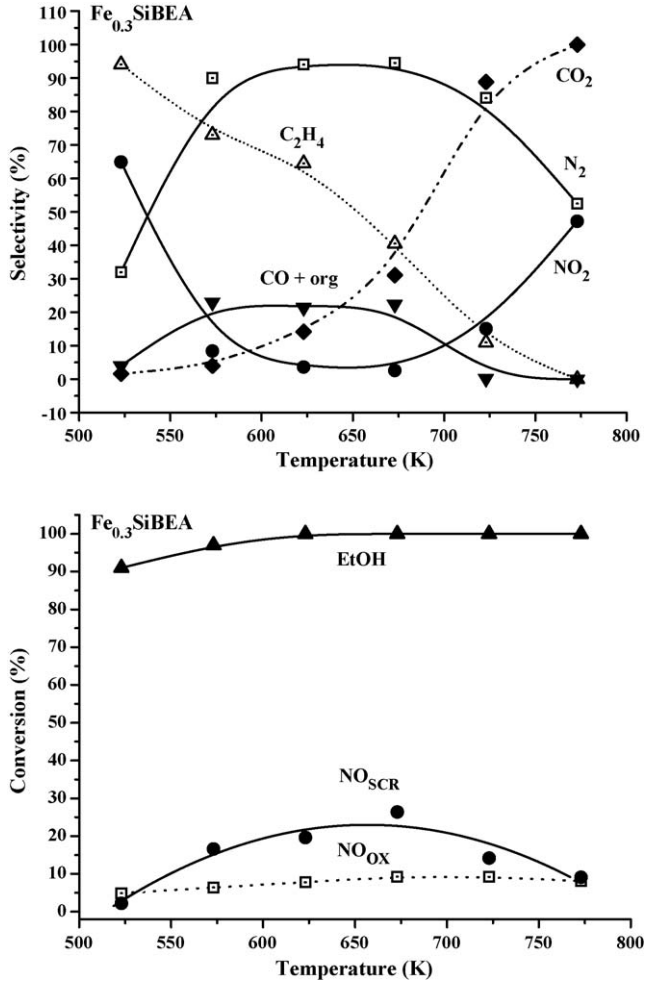

Fig. 10. Temperature-dependence of ethanol and NO conversions and product selectivities in SCR of NO by ethanol of $Fe_{0.3}$SiBEA.

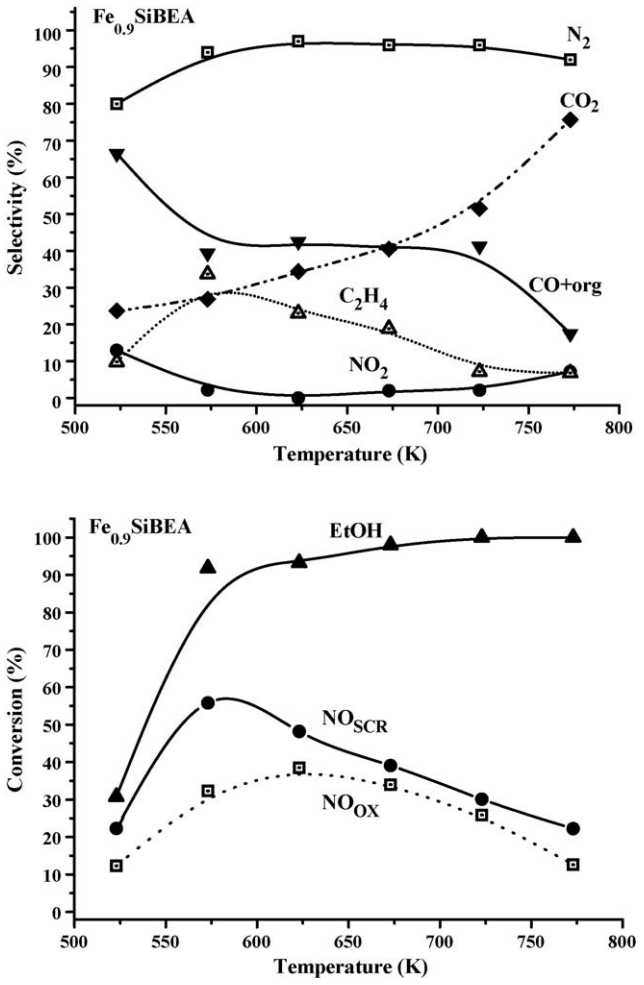

Fig. 11. Temperature-dependence of ethanol and NO conversions and product selectivities in SCR of NO by ethanol of $Fe_{0.9}$SiBEA.

As mentioned before, the SCR activity, measured as $\ln(1 - X_{NO})$ with X_{NO} conversion of NO measured at 525 K, increases linearly with Fe content for $Fe_{0.3}$SiBEA, $Fe_{0.9}$SiBEA and $Fe_{4.2}$SiBEA (Fig. 14). The SCR activity increases with the amount of tetrahedral Fe(III) species (see DR UV–vis data and Fig. 4). In contrast, $Fe_{3.6}$SiBEA, with mainly extra-framework iron oxide (DR UV–vis data), has an activity close to that of $Fe_{0.3}$SiBEA. The low activity of $Fe_{3.6}$SiBEA is related to the presence of a very small amount of tetrahedral Fe(III) ions (DR UV–vis data). The linear relationship in Fig. 14 evidence that Fe ions are well dispersed in the framework BEA zeolite as mononuclear (tetrahedral and/or octahedral) Fe(III) species. The straight-line dependence between Fe amount in Fe_xSiBEA catalysts (apart from $Fe_{3.6}$SiBEA) and the pseudo-first order reaction rate suggest, that the mononuclearity of Fe lattice species and not the Fe coordination number governs the overall activity. The latter, in the reaction condition, may be dynamically changed in the course of reagents adsorption. Only in the case, when the oxide-like Fe species (polynuclear Fe(III) species) are deposited inside the zeolite channels the activity drops substantially (as for $Fe_{3.6}$ SiBEA).

The present data suggest a "structure–properties" relationship similar to that reported earlier for Co_xSiBEA [43]. Indeed, $Fe_{0.3}$SiBEA and $Fe_{0.9}$SiBEA which mainly contain isolated tetrahedral Fe(III) ions exhibit an activity increasing with the amount of such ions.

However, at higher Fe content ($Fe_{4.2}$SiBEA), the activity increases but the selectivity toward N_2 decreases, especially above 650 K. The activity increase is related to the amount of isolated tetrahedral and/or octahedral Fe(III) ions and the selectivity decrease to extra-lattice FeO_x oligomers. Such oligomers lead to the full oxidation of ethanol by O_2. As in the case of Co_xSiBEA zeolites, extra-lattice oligomers enhance the oxidative activity of Fe_xSiBEA converting ethanol to CO_2 and NO to NO_2, in particular at high temperature, at which the concentration of reducing agents is

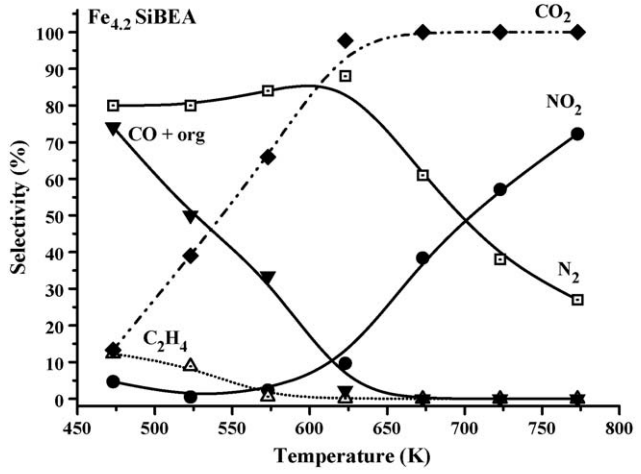

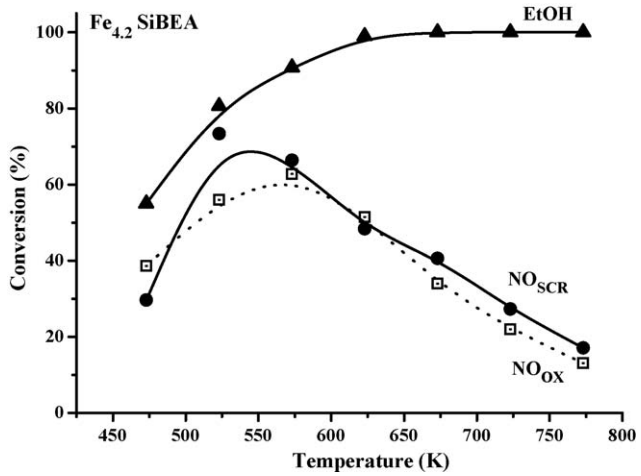

Fig. 12. Temperature-dependence of ethanol and NO conversions and product selectivities in SCR of NO by ethanol of $Fe_{4.2}$SiBEA.

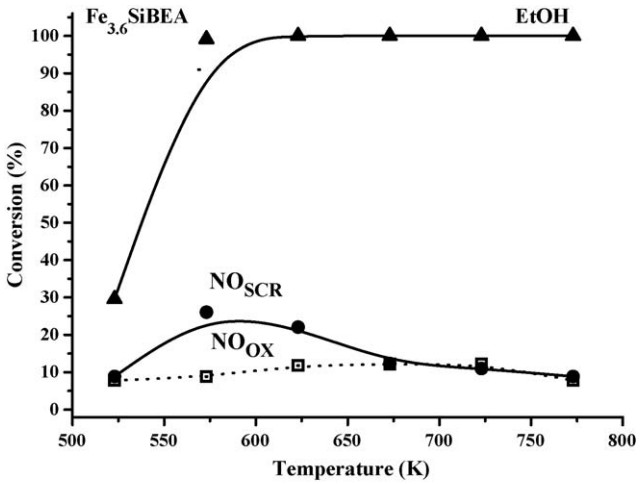

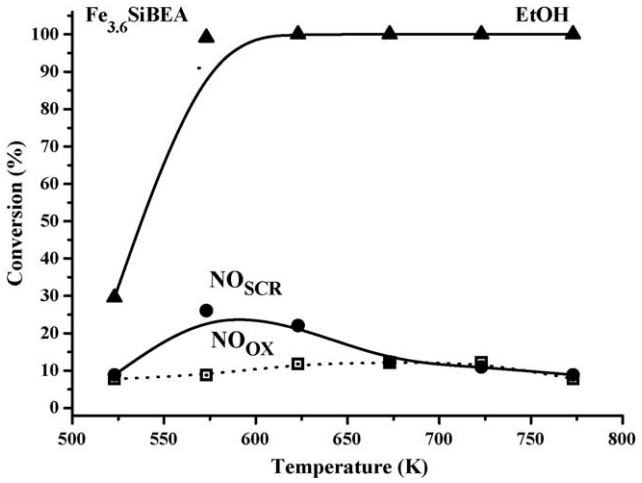

Fig. 13. Temperature-dependence of ethanol and NO conversions and product selectivities in SCR of NO by ethanol of $Fe_{3.6}$SiBEA.

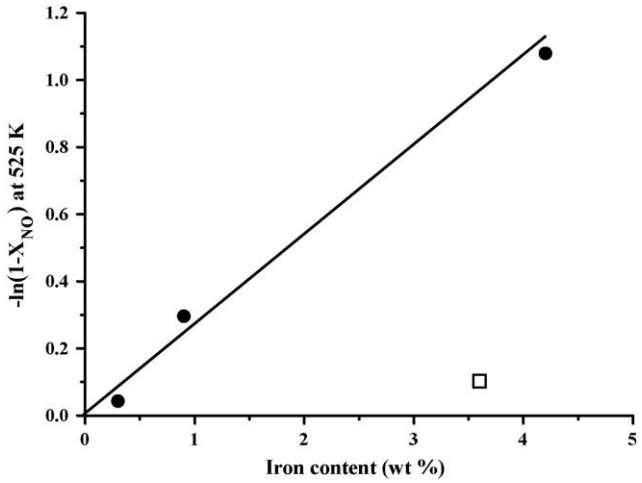

Fig. 14. Dependence of NO conversion (X_{NO}) on Fe content of $Fe_{0.3}$SiBEA, $Fe_{0.9}$SiBEA, $Fe_{4.2}$SiBEA (●), and $Fe_{3.6}$ SiBEA prepared in basic conditions (□).

Table 2
Dependence of the activity and selectivity on oxygen partial pressure at 623 K for SCR of NO by ethanol on $Fe_{0.9}$SiBEA zeolite.

Oxygen in He (vol.%)[a]	C_{EtOH}[b] (vol.%)	S_{CO}[c] (vol.%)	$S_{ethylene}$[d] (vol.%)	C_{NO}[e] (vol.%)	S_{N_2}[f] (vol.%)
7.5	95.5	31.8	5.2	26.3	86
5.0	96.5	41.1	7.9	41.2	89
2.5	94.0	38.1	12.9	45.4	92
1.25	94.5	38.4	13.4	47.7	96
0.82	92.7	30.0	17.4	56.9	97

[a] Oxygen in He = oxygen concentration (vol.%).
[b] C_{EtOH} = ethanol conversion (vol.%).
[c] S_{CO} = CO selectivity (vol.%).
[d] $S_{ethylene}$ = ethylene selectivity (vol.%).
[e] C_{NO} = NO conversion (vol.%).
[f] S_{N_2} = N_2 selectivity (vol.%).

much lower. Such catalytic behaviour of FeO_x oligomers and, especially α-Fe_2O_3-like structure was reported by Kumar et al. for SCR of NO by isobutane or ammonia on Fe-ZSM-5 [16]. Indeed, the presence of the iron oxide phase is detrimental to the SCR activity and cause nonselective oxidation of the reductant (isobutane and ammonia) at higher temperature. Moreover, such α-Fe_2O_3-like structure may block part of the inner zeolite channels diminishing the access and thus the overall catalytic activity.

As shown in Table 2 for $Fe_{0.9}$SiBEA at 623 K, the conversion of NO increases along with decreasing oxygen content in the reaction mixture, suggesting that the SCR of NO process does not depend on the ability of the catalyst to oxidize NO. It is also confirmed by the fact that the overall activity of Fe_xSiBEA catalysts in SCR of NO exceeds that in NO oxidation in the absence of ethanol (Figs. 10–13).

The data reported here show that the activity of Fe_xSiBEA in the oxidation of NO to NO_2 does not necessarily imply SCR activity, as postulated earlier [60,61]. The less NO oxidation is favored, the more SCR of NO toward N_2 on Fe_xSiBEA. According to our previous work [43], it is likely that the reaction mechanism involves the preliminary adsorption of NO that is oxidized by O_2 forming an adsorbed NO_x species (x = 2, 3) bound to a Fe(III) site.

Framework mononuclear Fe(III) species present in Fe_xSiBEA zeolite could activate ethanol molecule during the activated adsorption step and then forming an oxygenated intermediate. This active intermediate is probably responsible for SCR of NO toward N_2. According to the numerous literature data the first SCR step comprises the hydrogen abstraction from the hydrocarbon molecule. In our case it is hard to distinct between the hydrogen and hydroxyl group abstraction. The role of some active organic intermediates (nitro-compounds, acetonitrile, acetaldehyde) in the activation of NO molecule (unpublished results) not indicate clearly which bond undergoes scission during the first abstraction. On the basis of above mentioned experiments N-containing compounds as nitroethane and acetonitrile are very active and selective in the NO conversion to N_2 and seems to be one of the most probable SCR intermediates.

The SCR of NO into N_2 and NO oxidation into NO_2 seem to be competitive reactions and the ratio of N_2/NO_2 depends on the rate constants of both reactions and on reaction temperature. If we consider that at low temperature, reaction rate between adsorbed (NO_x) species and the organic molecule or desorption of reaction product is rate determining step, the secondary reaction between NO_2 (undergoing sequential adsorption) and adsorbed organic species has no effect on the overall kinetics but the N_2/NO_2 ratio depends on the kind of Fe(III) species present in Fe_xSiBEA zeolites.

4. Conclusions

The speciation of iron in Fe_xSiBEA zeolites investigated in this work allows to evidence the "structure–properties" relationship in the SCR of NO by ethanol.

Fe_xSiBEA zeolites (x = 0.3, 0.9 and 4.2 Fe wt%) prepared in acidic conditions (pH 2.5) by a two-step postsynthesis method allows to control the incorporation of iron into zeolite evidenced by XRD.

For low content ($Fe_{0.3}$SiBEA, $Fe_{0.9}$SiBEA), iron incorporated into the zeolite as Fe(III) ions generates Brønsted acidic sites as shown by FTIR of pyridine used as molecular probe.

The presence of framework tetrahedral Fe(III) ions is evidenced by Diffuse Reflectance UV–vis, XANES and EXAFS. For higher Fe content ($Fe_{4.2}$SiBEA), beside dominant tetrahedral Fe(III), octahedral Fe(III) ions are also present as shown by DR UV–vis, XPS and EXAFS.

In contrast, $Fe_{3.6}$SiBEA prepared in basic conditions (pH 10), exhibits mainly an extra-framework Fe(III) oxide phase.

The catalytic activity of Fe_xSiBEA in the SCR of NO by ethanol strongly depends on the speciation of iron and a structure–properties relationship has been evidenced.

$Fe_{0.3}$SiBEA and $Fe_{0.9}$SiBEA which mainly contain framework tetrahedral Fe(III) ions are active, with selectivity toward N_2 exceeding 90% for NO conversion from 25% to 55%. When additional octahedral Fe(III) are present ($Fe_{4.2}$SiBEA), the full oxidation of ethanol and NO by O_2 becomes important with CO_2 and NO_2, respectively appearing at the expenses of N_2. The NO conversion linearly depends on Fe concentration assuming a first order reaction. This suggests that octahedral Fe(III) species are well dispersed as confirmed by their XRD patterns.

The iron oxide phase seems to be quite inactive and the activity and selectivity for $Fe_{3.6}$SiBEA are probably governed by the small amount of tetrahedral Fe(III) ions present.

The lack of correlation between the activity in SCR of NO by ethanol and full oxidation of NO suggests that the two reactions are more competitive than sequential.

Further studies are underway to complement the description of the Fe sites active in the SCR of NO by *in situ* DRIFT and FTIR spectroscopy of adsorbed NO and CO.

Acknowledgments

S.D. gratefully acknowledges the CNRS (France) for financing his research position and J.J. acknowledges the GDRI CNRS-PAN for financing his stay in Paris.

References

[1] F. Kapteijn, J. Rodrigues-Mirasol, J.A. Moulijn, Appl. Catal. B 9 (1996) 25.
[2] J.A.Z. Pieterse, S. Booneveld, R.W. van den Brink, Appl. Catal. B 51 (2004) 215.
[3] G.D. Pirngruber, P.K. Roy, Catal. Today 110 (2005) 199.
[4] G.D. Pirngruber, P.K. Roy, Catal. Lett. 93 (2004) 75.
[5] H.Y. Chen, W.M.H. Sachtler, Catal. Today 42 (1998) 73.
[6] M. Kogel, R. Monnig, W. Schwieger, A. Tissler, T. Turek, J. Catal. 182 (1999) 470.
[7] J. Jia, K.S. Pillai, W.M.H. Sachtler, J. Catal. 221 (2004) 119.
[8] A. Ribera, I.W.C.E. Arends, S. De Vries, J.P. Sheldon, J. Catal. 195 (2000) 287.
[9] J. Perez-Ramirez, E.V. Kondratenko, J. Chem. Soc. Chem. Commun. (2003) 2152.
[10] Q. Kan, Z. Wu, R. Xu, X. Liu, S. Peng, J. Mol. Catal. 74 (1992) 223.

[11] R. Joyner, M. Stockenhuber, J. Phys. Chem. B 103 (1999) 5963.
[12] E.-M. El-Malki, R.A. van Santen, W.M.H. Sachtler, J. Catal. 196 (2000) 212.
[13] P. Kubanek, B. Wichterlova, Z. Sobalik, J. Catal. 211 (2002) 109.
[14] J. Perez-Ramirez, M.S. Kumar, A. Brückner, J. Catal. 218 (2003) 234.
[15] M. Yoshida, T. Nobukawa, S. Ito, K. Tomishige, K. Kunimori, J. Catal. 223 (2004) 454.
[16] M.S. Kumar, M. Schwidder, W. Grünert, A. Brückner, J. Catal. 227 (2004) 384.
[17] A. Guzman-Vergas, G. Delahay, B. Coq, Appl. Catal. B 42 (2003) 369.
[18] M. Mauvezin, G. Delahay, F. Kisslich, B. Coq, S. Kieger, Catal. Lett. 62 (1999) 41.
[19] D.M. Templeton, F. Ariese, R. Cornelis, L.G. Danielsson, H. Muntau, H.P. van Leeuwen, R. Lobinski, Pure Appl. Chem. 72 (2000) 1453.
[20] M. Iwamoto, H. Yahiro, K. Tanda, N. Mizuno, Y. Mine, S. Kagawa, J. Phys. Chem. 95 (1991) 3727.
[21] A. Penkova, K. Hadjiivanov, S. Dzwigaj, M. Che, J. Phys. Chem. C 111 (2007) 8623.
[22] S. Dzwigaj, M. Che, J. Phys. Chem. B 110 (2006) 12490.
[23] A. Mihaylova, K. Hadjiivanov, S. Dzwigaj, M. Che, J. Phys. Chem. B 110 (2006) 19530.
[24] S. Dzwigaj, M.J. Peltre, P. Massiani, A. Davidson, M. Che, T. Sen, S. Sivasanker, J. Chem. Soc. Chem. Commun. (1998) 87.
[25] S. Dzwigaj, M. Matsuoka, R. Franck, M. Anpo, M. Che, J. Phys. Chem. B 102 (1998) 6309.
[26] S. Dzwigaj, M. Matsuoka, M. Anpo, M. Che, J. Phys. Chem. B 104 (2000) 6012.
[27] S. Dzwigaj, L. Stievano, F.E. Wagner, M. Che, J. Phys. Chem. Solids 68 (2007) 1885.
[28] J.W. Cook, D.E.J. Sayers, Appl. Phys. 52 (1981) 5024.
[29] A.L. Ankudinov, B. Ravel, J.J. Rehr, S.D. Conradson, Phys. Rev. B 58 (1998) 7565.
[30] M.A. Camblor, A. Corma, J. Pérez-Pariente, Zeolites 13 (1993) 82.
[31] S. Dzwigaj, J. Janas, T. Machej, M. Che, Catal. Today 119 (2007) 133.
[32] S. Dzwigaj, T. Shishido, J. Phys. Chem. C 112 (2008) 5803.
[33] S. Dzwigaj, P. Massiani, A. Davidson, M. Che, J. Mol. Catal. A 155 (2000) 169.
[34] K. Gora-Marek, J. Datka, S. Dzwigaj, M. Che, J. Phys. Chem. B 110 (2006) 6763.
[35] S. Bordiga, R. Buzzoni, F. Geobaldo, C. Lamberti, E. Giamello, A. Zecchina, G. Leofanti, G. Petrini, G. Tozzola, G. Vlaic, J. Catal. 158 (1996) 486.
[36] H.H. Tippins, Phys. Rev. B 72 (1970) 279.
[37] P. Wu, T. Komatsu, T. Yashima, Micropor. Mesopor. Mater. 20 (1998) 139.
[38] L. Capek, V. Kreibich, J. Dedecek, T. Grygar, B. Wichterlova, Z. Sobalik, J.A. Martens, R. Brosius, V. Tokarova, Micropor. Mesopor. Mater. 80 (2005) 279.
[39] J. Perez-Ramirez, J.C. Groen, A. Brückner, M.S. Kumar, U. Bentrup, M.N. Debbagh, L.A. Villaescusa, J. Catal. 232 (2005) 318.
[40] M. Schwidder, S. Heikens, A. De Toni, S. Geisler, M. Berndt, A. Brückner, W. Grünert, J. Catal. 259 (2008) 96.
[41] P. Balle, B. Geiger, S. Kureti, Appl. Catal. B 85 (2009) 109.
[42] M.S. Kumar, M. Schwidder, W. Grünert, U. Bentrup, A. Brückner, J. Catal. 239 (2006) 173.
[43] J. Janas, T. Machej, J. Gurgul, R.P. Socha, M. Che, S. Dzwigaj, Appl. Catal. B 75 (2007) 239.
[44] K. Arishtirova, P. Kovacheva, A. Predoeva, Appl. Catal. A 243 (2003) 191.
[45] P. Kovacheva, K. Arishtirova, A. Predoeva, React. Kin. Catal. Lett. 79 (2003) 149.
[46] L.P. Oleksenko, Theor. Exp. Chem. 40 (2004) 331.
[47] M. Descostes, F. Mercier, N. Thromat, C. Beaucaire, M. Gautier-Soyer, Appl. Surf. Sci. 165 (2000) 288.
[48] H.W. Nesbitt, I.J. Muir, Geochim. Cosmochim. Acta 58 (1994) 4667.
[49] D.D. Hawn, B.M. Dekoven, Surf. Interf. Anal. 10 (1987) 63.
[50] P. Mills, J.L. Sullivan, J. Phys. D (Lond.) 16 (1983) 723.
[51] R.B. Borade, A. Clearfield, Micropor. Mater. 2 (1994) 167.
[52] C. Weidenthaler, B. Zibrowius, J. Ske, Y. Mao, B. Mienert, E. Bill, W. Schmidt, Micropor. Mesopor. Mater. 84 (2005) 302.
[53] C.R. Brundle, T.J. Chuang, K. Wandelt, Surf. Sci. 68 (1977) 459.
[54] J.H. Choy, J.B. Yoon, D.K. Kim, S.H. Hwang, Inorg. Chem. 34 (1995) 6524.
[55] T.E. Westre, P. Kennepohl, J.G. de Witt, B. Hedman, K.O. Hodgson, E.I. Solomon, J. Am. Chem. Soc. 119 (1997) 6297.
[56] S. Thomson, V. Luca, R. Howe, Phys. Chem. Chem. Phys. 1 (1999) 615.
[57] R.W.G. Wyckoff, 2nd ed., Crystal Structure, vol. 2, Interscience Publishers, New York, 1986.
[58] L. Pauling, S.B. Hendricks, J. Am. Chem. Soc. 47 (1925) 781.
[59] P. Fejes, K. Lazar, I. Marsi, A. Rockenbauer, L. Korecz, J.B. Nagy, S. Perathoner, G. Centi, Appl. Catal. A 252 (2003) 75.
[60] N.W. Cant, I.O.Y. Liu, Catal. Today 63 (2000) 133.
[61] R. Brosius, J.A. Martens, Top. Catal. 29 (2004).